

AN ACCURATE CENTROIDDING ALGORITHM FOR PSF RECONSTRUCTION

TIANHUAN LU¹, WENTAO LUO¹, JUN ZHANG¹, JIAJUN ZHANG¹, HEKUN LI¹, FUYU DONG¹, YINGKE LI¹, DEZI LIU², LIPING FU³, GUOLIANG LI⁴, ZUHUI FAN²

Draft version January 4, 2018

ABSTRACT

In this work, we present a novel centroiding method based on Fourier space Phase Fitting (FPF) for Point Spread Function (PSF) reconstruction. We generate two sets of simulations to test our method. The first set is generated by GalSim with elliptical Moffat profile and strong anisotropy which shifts the center of the PSF. The second set of simulation is drawn from CFHT i band stellar imaging data. We find non-negligible anisotropy from CFHT stellar images, which leads to ~ 0.08 scatter in unit of pixels using polynomial fitting method Vakili & Hogg (2016). And we apply FPF method to estimate the centroid in real space, this scatter reduces to ~ 0.04 in SNR = 200 CFHT-like sample. In low SNR (50 and 100) CFHT-like samples, the background noise dominates the shifting of the centroid, therefore the scatter estimated from different methods are similar. We compare polynomial fitting and FPF using GalSim simulation with optical anisotropy. We find that in all SNR (50, 100 and 200) samples, FPF performs better than polynomial fitting by a factor of ~ 3 . In general, we suggest that in real observations there are anisotropy which shift the centroid, and FPF method is a better way to accurately locate it.

Subject headings: techniques: image processing; methods: data analysis

1. INTRODUCTION

Point Spread Function (PSF) is one of the major systematics in weak lensing measurement. It introduces both multiplicative bias and additive bias. There are numerous methods in literature devoted to correcting PSF effects (Kaiser et al. 1995; Bertin & Arnouts 1996; Maoli et al. 2000; Rhodes et al. 2000; van Waerbeke 2001; Bernstein & Jarvis 2002; Bridle et al. 2002; Refregier 2003; Bacon & Taylor 2003; Hirata & Seljak 2003; Heymans et al. 2005; Zhang 2010, 2011; Bernstein & Armstrong 2014; Zhang et al. 2015; Luo et al. 2017). Lensfit (Miller et al. 2007, 2013; Kitching et al. 2008) applies a Bayesian based model-fitting approach; BFD (Bayesian Fourier Domain) method (Bernstein & Armstrong 2014) carries out Bayesian analysis in the Fourier domain, using the distribution of unlensed galaxy moments as a prior, and the Fourier_Quad method developed by (Zhang 2010, 2011; Zhang et al. 2015; Zhang 2016) uses image moments in the Fourier Domain.

Many simulations are generated to test the accuracy of various methods, e.g. STEP (Shear TESTING Program) (Heymans et al. 2006; Massey et al. 2007a), Great08 (Bridle et al. 2009), Great 10 (Kitching et al. 2010), GREAT3 (Mandelbaum et al. 2014) or Kaggle – the dark matter mapping competition⁵. Other independent softwares, such as SHERA (Mandelbaum et al. 2012, hereafter M12), have also been designed for specific

surveys. But most of those simulations assume that the PSF is perfectly known, which is not the case in reality. PSF at the position of galaxy must be reconstructed using nearby star images.

In GREAT10 star challenge (Kitching et al. 2013), multiple PSF reconstruction methods has been tested, e.g. PSFEx (Bertin 2011), PCA+Krigging (Li, Xin, & Cui 2013), Gaussianlets (Li, Xin, & Cui 2013), B-spline (Gentile et al. 2013), Inverse Distance Weighting (IDW), Radial Basis Function(RBF), and Krigging (Bergé et al. 2012) etc. Especially, Lu et al. (2016) tested various interpolation methods to interpolate the PSF power spectrum for Fourier_Quad shear estimator (Zhang et al. 2015), which achieves $< 1\%$ level accuracy in GREAT3 simulation.

As for estimating the centroid of stellar images, a recent work by Vakili & Hogg (2016) claims that simple polynomial fitting works very well and close to saturate the Cramér-Rao lower bound, while moment-based method does not deliver reliable centroid estimation. Our method, though, based on fitting the phase slope in Fourier space, not only provide better centroid estimation in terms of scatter, but also automatically shift the centroid to the center of a postage-stamp image after inverse Fourier transformation.

We describe our method along with polynomial fitting, in Sec. 2. In Sec. 3, we describe the simulations to test our method. The results are shown in Sec. 4. We summarize and conclude in Sec. 5.

2. METHOD

In this section, we describe our centeroid measurement method along with polynomial fitting method with a Gaussian smooth kernel.

2.1. Fourier space Phase Fitting (FPF)

arXiv:1801.01015v1 [astro-ph.IM] 26 Dec 2017

¹Department of Physics and Astronomy, Shanghai Jiao Tong University, Shanghai, 200240, China; E-mail: njpipeorgan@sjtu.edu.cn, wentao.luo82@sjtu.edu.cn

²Department of Astronomy, School of Physics, Peking University, Beijing 100871, China

³The Shanghai Key Lab for Astrophysics, Shanghai Normal University, Shanghai 200234, China

⁴Purple Mountain Observatory, Chinese Academy of Sciences, Nanjing, 210000, China

⁵Supported by NASA & the Royal Astronomical Society.

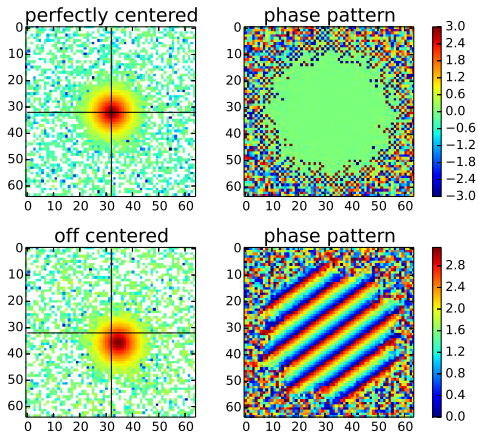


FIG. 1.— Upper left: perfectly centered star image; Upper right: the phase at each (k_x, k_y) ; Lower left: off centered star image; Lower right: phase pattern caused by off centering effect.

Given an image $I(\mathbf{x})$ and its centroid \mathbf{x}_c . The Fourier transformation of the image is simply

$$f(\mathbf{k}) = \frac{1}{2\pi} \iint I(\mathbf{x}) e^{-i\mathbf{k}\cdot\mathbf{x}} d\mathbf{x}, \quad (1)$$

where $f(\mathbf{k})$ can be written as

$$f(\mathbf{k}) = |f(\mathbf{k})| e^{i\angle f(\mathbf{k})}, \quad (2)$$

with $\angle(f)$ as the phase. Given that the centroid of a noise free PSF image $I(\mathbf{x})$ is defined as

$$\mathbf{x}_c := \frac{\iint \mathbf{x} I(\mathbf{x}) d\mathbf{x}}{\iint I(\mathbf{x}) d\mathbf{x}}, \quad (3)$$

we find that the centroid \mathbf{x}_c in real space corresponds to the slope of phase near $\mathbf{k} = 0$, i.e.

$$\mathbf{x}_c = -\nabla \angle f(0). \quad (4)$$

The proof is shown in the appendix.

In the case that the image is symmetric about the centroid, which is usually the case in the vicinity of the centroid and the image value is real. Then according to the Fourier transformation properties we can deduce that

$$f(\mathbf{k}) = f(-\mathbf{k}) = f^*(\mathbf{k}). \quad (5)$$

As a result, $f(\mathbf{k})$ is also a real function, meaning the imaginary part vanishes and the phase function is zero. Any anisotropy can further introduce non-zero imaginary part, which can be reflected by the phase.

Fig. 1 gives an example of how off-center affect the phase pattern in Fourier space. The phase will be zero if the image is perfectly centered, while there will be stripe pattern caused by off centering effect.

After discretization, the derivative becomes a minimization problem:

$$\chi^2 = \sum_{\mathbf{k}} w(\mathbf{k}) \left[\angle \left(f(\mathbf{k}) e^{-i\phi(\mathbf{k})} \right) \right]^2 \quad (6)$$

where $f(\mathbf{k}) = f_p(\mathbf{k}) + f_n(\mathbf{k})$ is the Fourier transform of the PSF ($f_p(\mathbf{k})$) with noise ($f_n(\mathbf{k})$), and $\phi(\mathbf{k})$ is the modeled phase pattern of $f(\mathbf{k})$, which depends on the PSF ($f(\mathbf{k})$), the centroid (\mathbf{x}_c). The observed image is

a matrix with real values, so its Fourier transformation satisfies the conditions that are $f(-\mathbf{k}) = f^*(\mathbf{k})$ and $\phi(-\mathbf{k}) = -\phi(\mathbf{k})$.

For a symmetric PSF, the phase is simply related with the centroids linearly,

$$\phi = k_x x_c + k_y y_c. \quad (7)$$

Nevertheless, the higher order anisotropy that shifts centroids, should be fitted with higher order (here we apply 3rd order) polynomial to capture this effect,

$$\phi = k_x x_c + k_y y_c + \alpha_1 k_x^3 + \alpha_2 k_x^2 k_y + \alpha_3 k_x k_y^2 + \alpha_4 k_y^3, \quad (8)$$

where $\{\alpha_1, \alpha_2, \alpha_3, \alpha_4\}$ are free parameters.

In the appendix, We show that the weights bearing the analytical form

$$w(\mathbf{k}) = \begin{cases} \frac{2|f(\mathbf{k})|^2}{|f_n(\mathbf{k})|^2}, & |f_n(\mathbf{k})| \ll |f_p(\mathbf{k})| \\ 0, & |f_n(\mathbf{k})| \approx |f_p(\mathbf{k})| \end{cases} \quad (9)$$

can out-weight the noise while preserve as many data points as possible for the fitting.

2.2. Polynomial fitting method

We follow Vakili & Hogg (2016) and apply a fixed Gaussian kernel

$$k(x) = \frac{1}{2\pi w^2} \exp(-x^2/2w^2). \quad (10)$$

where w is 1.2 pixels given that the PSF FWHM is 2.8 pixels, to smooth the image before fitting the centroids with 2D polynomial

$$P(x, y) = a + bx + cy + dx^2 + exy + fy^2. \quad (11)$$

Only the central 3×3 patch around the brightest pixels are used to solve the coefficients $X = \{a, b, c, d, e, f\}$. The design matrix A can be constructed as

$$A = \begin{pmatrix} 1 & x_1 & y_1 & x_1^2 & x_1 y_1 & y_1^2 \\ 1 & x_2 & y_2 & x_2^2 & x_2 y_2 & y_2^2 \\ \vdots & \vdots & \vdots & \vdots & \vdots & \vdots \\ 1 & x_9 & y_9 & x_9^2 & x_9 y_9 & y_9^2 \end{pmatrix}. \quad (12)$$

Then the coefficients can be determined by solving

$$X = (A^T A)^{-1} A^T Z \quad (13)$$

where Z is the pixels of the flattened 3×3 patch. The centroids can be then determined by those coefficients.

$$\begin{pmatrix} x_c \\ y_c \end{pmatrix} = D^{-1} \begin{pmatrix} -b \\ -c \end{pmatrix}, \quad (14)$$

where $D = \begin{pmatrix} 2d & e \\ e & 2f \end{pmatrix}$, is the curvature matrix,

3. SIMULATIONS

We simulated two sets of images, one uses GalSim (Rowe et al. 2015) and the other is based on Principal Components (PCs) decomposed from CFHT w2 stellar images. The GalSim simulation provides a set of optical effects. The CFHT simulation is for exploring how much shifts caused by the anisotropy in real surveys.

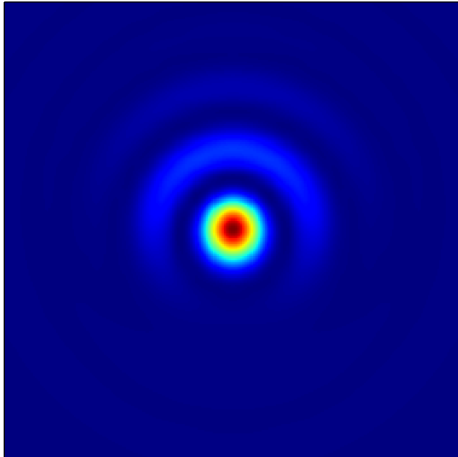


FIG. 2.— This figure demonstrates the effect of coma with 0.07 deviation in y -direction from GalSim.

3.1. GalSim stellar image

We use GalSim to simulate 3 sets of star images with different signal to noise ratio: SNR ~ 50 , SNR ~ 100 and SNR ~ 200 . The SNR is not strictly 50, 100 or 200 due to the fact that we simulate the images using Exposure Time Calculator (ETC) from a uniform magnitude distribution centered at each SNR.

We apply Moffat profile for all the stellar images, and uniform distribution for the r_d and β in

$$I(r) = \left(1 + \frac{r^2}{r_d^2}\right)^{-\beta}, \quad (15)$$

where $I(r)$ is the 2D brightness distribution. After we generate the stellar images, we shift the centers using two uniform distributions from -0.5 to 0.5 to each image as input centroid value. Then we convolve the images with optical anisotropy effect coma as shown in Fig. 2. We exaggerate this effect for better illustration, in fact, it is hard to be noticed by visual inspection. Finally we add Gaussian noise using GalSim to simulate difference SNR stellar images. Noise and randomly oriented optical anisotropy contribute more dispersion to the centroid of the image.

3.2. CFHT w2 stellar image

In real observations, atmospheric seeing dilutes the observed objects and introduce extra ellipticity and shift on centroid. The background sky also shifts the centroid randomly. For high SNR images, the centroid-shifting mechanism is dominated by atmospheric seeing. An accurate centroid estimation method should be designed to capture this shifting and correct for it.

In this simulation, we focus on testing this high order centroid shifting effect based on real data from CFHTLens survey field w2, which contains 7 exposures, with 10 minutes exposure for each.

The procedure of this simulation is described as follows:

- Select all the stellar images with SNR > 100 and without saturation from CFHT w2 area, there are $\sim 600,000$ stars in total.

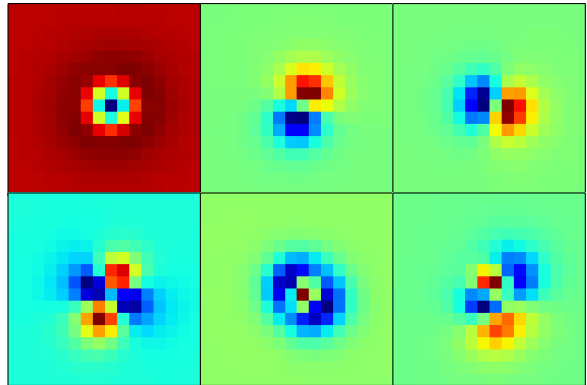


FIG. 3.— The first six Principal Components(PCs) from CFHT w2 stellar images.

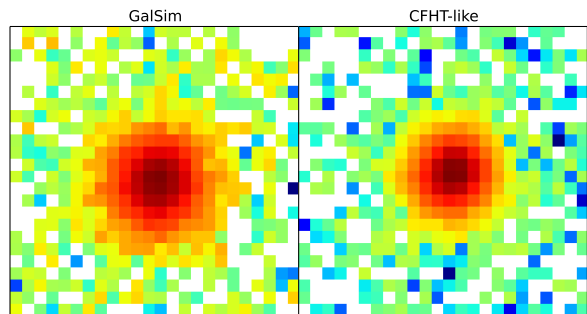


FIG. 4.— The left panel is the PSF simulated by GalSim and the right panel is the CFHT-like PSF.

- Extract components using PCA without centroiding.
- Generate 10,000 stellar images using the first 16 PCs, the coefficients of the PCs are randomly drawn from the parent distribution of the original images.
- Calculate the centroid using brightness weighted moments using

$$\mathbf{x}_0 = \frac{\iint \mathbf{x} I(\mathbf{x}) d\mathbf{x}}{\iint I(\mathbf{x}) d\mathbf{x}}. \quad (16)$$

to be the reference. This can be considered as the real input center when there is no noise.

The first 6 PCs decomposed from CFHT w2 stellar images are shown in Fig. 3. We preserve the dipoles by not centroiding the postage stamp images so that the asymmetry can be directly reconstructed by the dipoles.

We display the images from two simulations in Fig. 4. The right panel is the PSF from GalSim simulation and the left one is CFHT-like simulation. Despite of the anisotropy effect added to GalSim PSFs, we still can not observe its existence by visual inspection.

4. RESULTS

We demonstrate the performance of three centroiding methods Fig. 5, i.e. polynomial fitting, 1st order phase fitting and 3rd order phase fitting based on two simulations. The top three panels show the results from GalSim simulation, the bottom three are from CFHT-like simulation. From left to right, the SNR = 50, 100, 200 respectively.

In general, 1st order FPF is already better than polynomial fitting in both simulations, and 3rd FPF is significantly improves the centroid estimation. In CFHT-like SNR = 50 simulation, all three methods perform similarly due to the fact that the sky background noise dominates the scatter budget. The quantitative comparison is listed in Table. 1.

TABLE 1
THE CENTROIDING SCATTER COMPARISON IN UNIT OF PIXEL.

| Simulation | SNR | Polynomial | 1st order FPF | 3rd order FPF |
|------------|-----|------------|---------------|---------------|
| Galsim | 50 | 0.3569 | 0.2350 | 0.1559 |
| | 100 | 0.3525 | 0.2336 | 0.1127 |
| | 200 | 0.3562 | 0.2396 | 0.1105 |
| CFHT-like | 50 | 0.0877 | 0.0814 | 0.0891 |
| | 100 | 0.0762 | 0.0601 | 0.0495 |
| | 200 | 0.0740 | 0.0592 | 0.0377 |

In GalSim simulation, where the optical anisotropy dominates the scatter budget, the scatter from 3rd order FPF is ~ 3 times smaller than that from polynomial fitting in all SNR branches.

In CFHT-like simulation, the performance of three methods are similar in SNR = 50 branch. For SNR = 100 branch, which are often used in real analysis, the scatter from 3rd order FPF is ~ 1.5 smaller than that from polynomial fitting. This difference expands to ~ 2.0 for SNR = 200 branch.

In the CFHT-like simulation, the performance of three methods are similar in SNR = 50 branch. As we increase SNR to 100, which is closer to those in real measurements, the scatter from 3rd order FPF is ~ 1.5 smaller than that from polynomial fitting. This difference expands to ~ 2.0 for SNR = 200 branch. As the effect of noise drops, 3rd order FPF has a better and better per-

formances relative to polynomial fitting, due to its ability to accurately capture higher order anisotropy features.

It can be further illustrated by the GalSim simulation, where higher order anisotropy dominates the scatter budget. In all SNR branches, the scatter from 3rd order FPF is ~ 3 times smaller than that from polynomial fitting.

5. SUMMARY AND DISCUSSION

Centroiding is the first and important procedure for PSF reconstruction. An accurate PSF reconstruction further affects shear measurement. We develop our centroid estimation method in Fourier space – 3rd order FPF.

In GalSim simulation, the centroiding shift is dominated by optical anisotropy. The scatter of 3rd order FPF are smaller than polynomial fitting method by a factor of ~ 2 to ~ 3 , from SNR = 50 to SNR = 200 branch.

In CFHT-like simulation, where the higher order anisotropy is much smaller than GalSim simulation, we found that for the SNR = 50 images, background noise dominate the scatter, while for the SNR = 200, optical anisotropy play a major role for this scatter. Therefore 3rd order FPF performs similarly in SNR = 50 branch, but with half the scatter of polynomial fitting method in SNR = 200 branch.

Therefore, we conclude that 3rd order FPF method is so far the most accurate estimation in centroiding. The scatter caused by noise can not well corrected for any methods, but for scatter introduced by optical anisotropies, 3rd order FPF can capture the shift precisely. This is very important for weak lensing measurements.

This work was supported by the following programs; NSFC (Nos. 11503064), Shanghai Natural Science Foundation, Grant No. 15ZR1446700. JZ is supported by the NSFC grants (11673016, 11433001, 11621303) and the National Key Basic Research Program of China (2015CB857001). L.P.F. acknowledges the support from NSFC grant 11333001 and 11673018, STCSM grants 13JC1404400 and 16R1424800, SHNU grant DY1201603.

This work was also supported by the High Performance Computing Resource in the Core Facility for Advanced Research Computing at Shanghai Astronomical Observatory.

REFERENCES

- Bacon, D. J., & Taylor, A. N. 2003, MNRAS, 344, 1307
 Bergé, J., Price, S., Amara, A., & Rhodes, J. 2012, MNRAS, 419, 2356
 Bertin, E. 2011, Astronomical Data Analysis Software and Systems XX, 442, 435
 Bernstein, G. M., & Jarvis, M. 2002, AJ, 123, 583
 Bernstein, G. M. 2009, ApJ, 695, 652
 Bernstein, G. M., & Armstrong, R. 2014, MNRAS, 438, 1880
 Bertin, E., & Arnouts, S. 1996, A&AS, 117, 393
 Bridle, S. L., Kneib, J.-P., Bardeau, S., & Gull, S. F. 2002, The Shapes of Galaxies and their Dark Halos, 38
 Bridle, S., Shawe-Taylor, J., Amara, A., et al. 2009, Annals of Applied Statistics, 3, 6
 Gentile, M., Courbin, F., & Meylan, G. 2013, A&A, 549, A1
 Heymans, C., Brown, M., Heavens, A., et al. 2004, MNRAS, 347, 895
 Heymans, C., Brown, M. L., Barden, M., et al. 2005, MNRAS, 361, 160
 Heymans, C., Van Waerbeke, L., Bacon, D., et al. 2006, MNRAS, 368, 1323
 Hirata, C., & Seljak, U. 2003, MNRAS, 343, 459
 Kaiser, N., Squires, G., & Broadhurst, T. 1995, ApJ, 449, 460
 Kaiser, N. 2000, ApJ, 537, 555
 Kitching, T. D., Miller, L., Heymans, C. E., van Waerbeke, L., & Heavens, A. F. 2008, MNRAS, 390, 149
 Kitching, T., Balan, S., Bernstein, G., et al. 2010, arXiv:1009.0779
 Kilbinger, M., Fu, L., Heymans, C., et al. 2013, MNRAS, 430, 2200
 Li, G., Xin, B., & Cui, W. 2013, Astrophysics from Antarctica, 288, 306
 Lu, T., Zhang, J., Dong, F., et al. 2016, arXiv:1610.09828
 Luo, W., Yang, X., & Zhang, J. 2017, ApJ, 836, 1
 Kitching, T. D., Rowe, B., Gill, M., et al. 2013, ApJS, 205, 12
 Mandelbaum, R., Hirata, C. M., Leauthaud, A., Massey, R. J., & Rhodes, J. 2012, MNRAS, 420, 1518
 Mandelbaum, R., Rowe, B., Bosch, J., et al. 2014, ApJS, 212, 5
 Mandelbaum, R., Rowe, B., Armstrong, R., et al. 2015, MNRAS, 450, 2963
 Maoli, R., Mellier, Y., van Waerbeke, L., et al. 2000, The Messenger, 101, 10

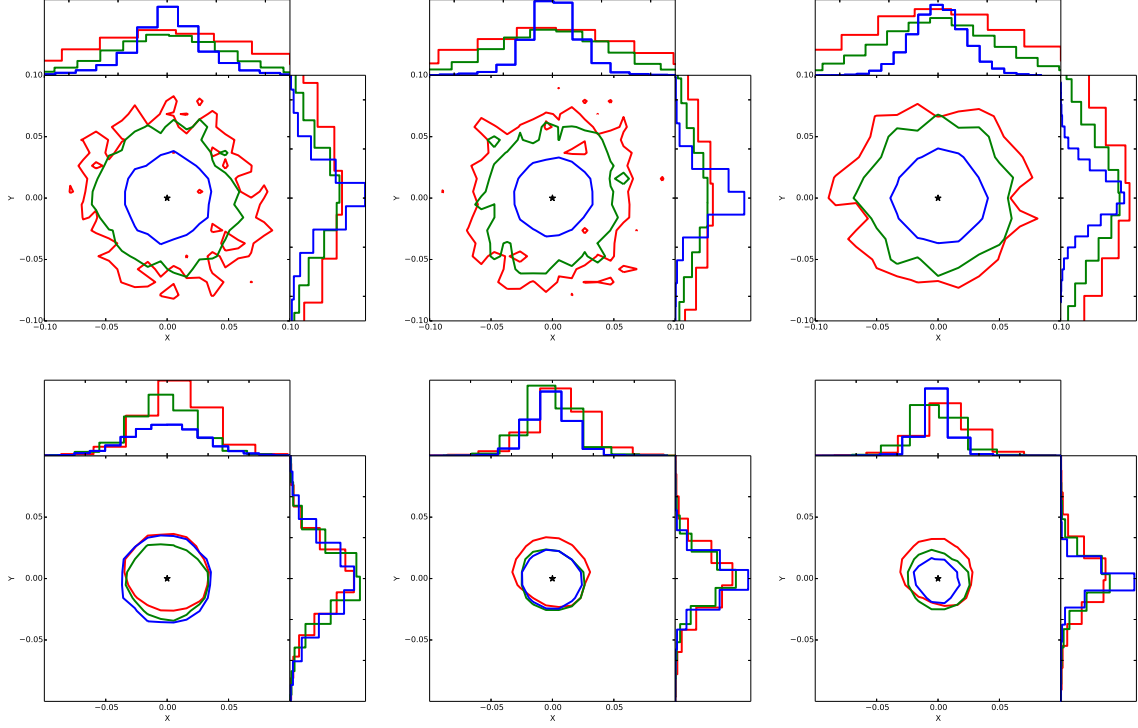


FIG. 5.— Upper panel: Galsim simulation; Lower panel: CFHT w2 simulation. The red, green and blue lines denote one sigma scatter of polynomial, 1st order FPF and 3rd order FPF centroiding method. The histograms are the residual distribution of centroids in x,y directions respectively.

Massey, R., Rhodes, J., Leauthaud, A., et al. 2007a, *ApJS*, 172, 239
 Miller, L., Kitching, T. D., Heymans, C., Heavens, A. F., & van Waerbeke, L. 2007, *MNRAS*, 382, 315
 Miller, L., Heymans, C., Kitching, T. D., et al. 2013, *MNRAS*, 429, 2858
 Refregier, A. 2003, *ARA&A*, 41, 645
 Refregier, A., Amara, A., Kitching, T. D., et al. 2010, [arXiv:1001.0061](https://arxiv.org/abs/1001.0061)
 Rhodes, J., Refregier, A., & Groth, E. J. 2000, *ApJ*, 536, 79
 Rhodes, J. D., Massey, R. J., Albert, J., et al. 2007, *ApJS*, 172, 203

Rowe, B. T. P., Jarvis, M., Mandelbaum, R., et al. 2015, *Astronomy and Computing*, 10, 121
 Vakili, M., & Hogg, D. W. 2016, [arXiv:1610.05873](https://arxiv.org/abs/1610.05873)
 van Waerbeke, L. 2001, *Cosmological Physics with Gravitational Lensing*, 165
 Zhang, J. 2010, *MNRAS*, 403, 673
 Zhang, J. 2011, *JCAP*, 11, 041
 Zhang, J., Luo, W., & Foucaud, S. 2015, *JCAP*, 1, 024
 Zhang, J. 2016, *National Science Review*, 3, 159-164

APPENDIX

A. CENTROID OF A PSF IMAGE IN FOURIER SPACE

First, we calculate the derivative of $f(\mathbf{k})$ with respect to k_x at $\mathbf{k} = 0$:

$$\begin{aligned}
 \left. \frac{\partial}{\partial k_x} \right|_{\mathbf{k}=0} f(\mathbf{k}) &= \left. \frac{\partial}{\partial k_x} \right|_{\mathbf{k}=0} \left\{ \frac{1}{2\pi} \iint I(\mathbf{x}) e^{-i\mathbf{k}\cdot\mathbf{x}} d\mathbf{x} \right\} \\
 &= \left. \frac{\partial}{\partial k_x} \right|_{k_x=0} \left\{ \frac{1}{2\pi} \iint I(x, y) e^{-ik_x x} dx dy \right\} \\
 &= \frac{1}{2\pi} \iint I(x, y) \left. \frac{\partial}{\partial k_x} \right|_{k_x=0} e^{-ik_x x} dx dy \\
 &= -\frac{i}{2\pi} \iint I(x, y) x dx dy \\
 &= -ix_c \frac{1}{2\pi} \iint I(x, y) dx dy, \\
 &= -if(0) x_c.
 \end{aligned} \tag{A1}$$

Next, we related the derivative of $f(\mathbf{k})$ with respect to k_x with that of $\angle f(\mathbf{k})$:

$$\begin{aligned} \frac{\partial}{\partial k_x} \Big|_{\mathbf{k}=0} f(\mathbf{k}) &= \frac{\partial}{\partial k_x} \Big|_{\mathbf{k}=0} \left\{ |f(\mathbf{k})| e^{i\angle f(\mathbf{k})} \right\} \\ &= |f(0)| e^{i\angle f(0)} \left(i \frac{\partial}{\partial k_x} \Big|_{\mathbf{k}=0} \angle f(\mathbf{k}) \right) + \frac{\partial f(0)}{\partial k_x} e^{i\angle f(0)} \\ &= i f(0) \frac{\partial}{\partial k_x} \Big|_{\mathbf{k}=0} \angle f(\mathbf{k}) \end{aligned} \quad (\text{A2})$$

Compare Eqn.(A1) with Eqn.(A2), we find

$$x_c = - \frac{\partial}{\partial k_x} \Big|_{\mathbf{k}=0} \angle f(\mathbf{k}), \quad (\text{A3})$$

and similarly,

$$y_c = - \frac{\partial}{\partial k_y} \Big|_{\mathbf{k}=0} \angle f(\mathbf{k}). \quad (\text{A4})$$

Thus, we get

$$\mathbf{x}_c = -\nabla \angle f(0). \quad (\text{A5})$$

B. WEIGHTS IN FOURIER PHASE FITTING

Suppose the Fourier transform of the noise free PSF is $f_p(\mathbf{k})$, and the noise has magnitude $|f_n(\mathbf{k})|$ and random phase. Given $f = f_p + f_n$, we can deduce the scatter of $\angle f$ in terms of its variance.

When $|f_n| \ll |f_p|$ (without loss of generality, we let $f_p \in \mathbb{R}$),

$$\begin{aligned} \text{Var}(\angle f) &= \langle (\angle f - \langle \angle f \rangle)^2 \rangle \\ &= \langle (\angle(f_p + f_n) - \angle f_p)^2 \rangle \\ &= \left\langle \left(\text{Im}(f_n) \nabla_{\text{Im}} \angle f|_{f=f_p} \right)^2 \right\rangle \\ &= \frac{1}{2} |f_n|^2 \left(\frac{df^{-1}}{df} \Big|_{f=f_p} \right)^2 \\ &= \frac{|f_n|^2}{2 |f_p|^2}, \end{aligned} \quad (\text{B1})$$

where ∇_{Im} denotes the directional derivative along the imaginary part.

The weights should be inversely proportional to the variances. We take

$$w(\mathbf{k}) = \text{Var}(\angle f)^{-1} = \frac{2 |f_p|^2}{|f_n|^2} \approx \frac{2 |f|^2}{|f_n|^2}. \quad (\text{B2})$$

When $|f_n| \approx |f_p|$, the scatters of $\angle f$ are so large that such pixels do not provide useful information of $\angle f_p$. Thus we take

$$w(\mathbf{k}) = 0. \quad (\text{B3})$$